Appendix 1: Liver CT scan protocol

Liver CT examinations were obtained using various multidetector row CT scanners. The training set included CT scans acquired on Ingenuity CT (Philips Healthcare, Best, Netherlands; n=51), iCT 256 (Philips Healthcare; n=23), Discovery CT750 HD (GE Healthcare, Milwaukee, WI, USA; n=21), and SOMATOM Definition (Siemens Healthineers; n=48). For the validation set, scans were obtained using Ingenuity CT (Philips Healthcare; n=16), Discovery CT750 HD (GE Healthcare; n=2), and SOMATOM Definition (Siemens Healthineers; n=20).

All scans were performed according to our institution's routine liver CT protocol. After acquisition of precontrast images, intravenous nonionic contrast medium [iobitridol (Xenetix 350, Guerbet, Villepinte, France) or iohexol (Bonorex 350, Central Medical Service, Seoul, Korea)] was injected at a dose of 1.6 mL/kg at a rate of 3–5 mL/sec, followed by a 20–40 mL saline flush using an automatic power injector. Using the bolus tracking technique, arterial phase images were obtained with a scan delay of 17–19 seconds after reaching a threshold enhancement of 100 Hounsfield units (HUs) in the distal thoracic aorta. Portal venous phase imaging was performed with a delay of 45–50 seconds, and delayed phase images were acquired 180 seconds after the start of contrast administration. Scans were reconstructed with a slice thickness of 2.5–3.0 mm and a peak voltage of 100 kVp using filtered back projection algorithms. The scan range extended from the dome of the diaphragm to the iliac crest. During the portal venous phase, coverage was further extended caudally to include the pelvic cavity.

https://dx.doi.org/10.21037/jgo-2025-aw-919

Appendix 2: Detailed image review process

The image review process was conducted in two steps: the first step involved candidate lesion identification, and the second step employed blinded consensus review to confirm lesions meeting NAPH criteria for the final study population.

Step 1: preliminary lesion identification

An experienced abdominal radiologist conducted an unblinded preliminary review to identify potential NAPH lesions on CT. This coordinating radiologist had access to both CT and MRI findings to establish candidate lesions and determine MRI-based reference diagnoses. Lesion sizes were measured during this preliminary assessment. When multiple lesions were present in a single patient, up to three lesions were selected using a prioritization strategy: HCC-suggestive lesions were selected first, followed by lesions with the largest diameter. Lesions with other benign diagnoses on MRI, such as hemangiomas or focal nodular hyperplasia-like nodules, were excluded to maintain focus on the differentiation between small HCC and vascular pseudolesions. This preliminary review resulted in 336 NAPH candidate lesions from 212 patients marked for subsequent consensus evaluation.

Step 2: consensus NAPH confirmation

Three fellowship-trained abdominal radiologists performed a blinded consensus review of the candidate lesions, with no access to MRI findings or preliminary diagnoses. The reviewers evaluated all CT phases using both filtered back projection and iterative reconstruction images, reflecting routine clinical practice protocols. Lesions were confirmed as NAPH if they demonstrated APHE without washout, enhancing capsule, or other definitive features that would suggest a specific diagnosis. Lesions with wedge-shaped morphology were excluded as they did not meet the nodular definition of NAPH. For confirmed NAPH lesions, lesion location (subcapsular *vs.* non-subcapsular) was documented for subsequent analysis.

https://dx.doi.org/10.21037/jgo-2025-aw-919

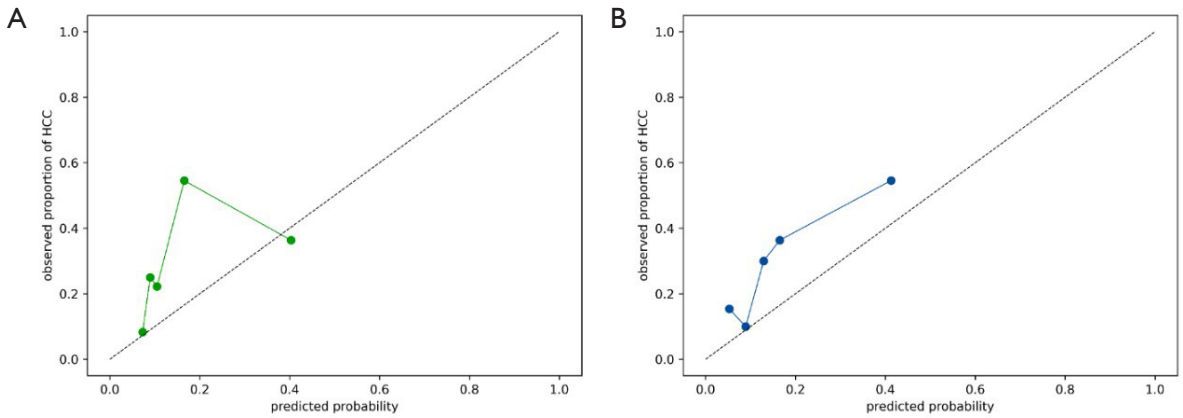

Figure S1 Calibration plots of the radiomics model and combined models in the validation set. Calibration plots of the radiomics model (A) and the combined model (B) in the validation set. The plots show the relationship between predicted probabilities and the observed proportions of HCC across quantile-based bins. The dashed diagonal line represents perfect calibration. HCC, hepatocellular carcinoma.

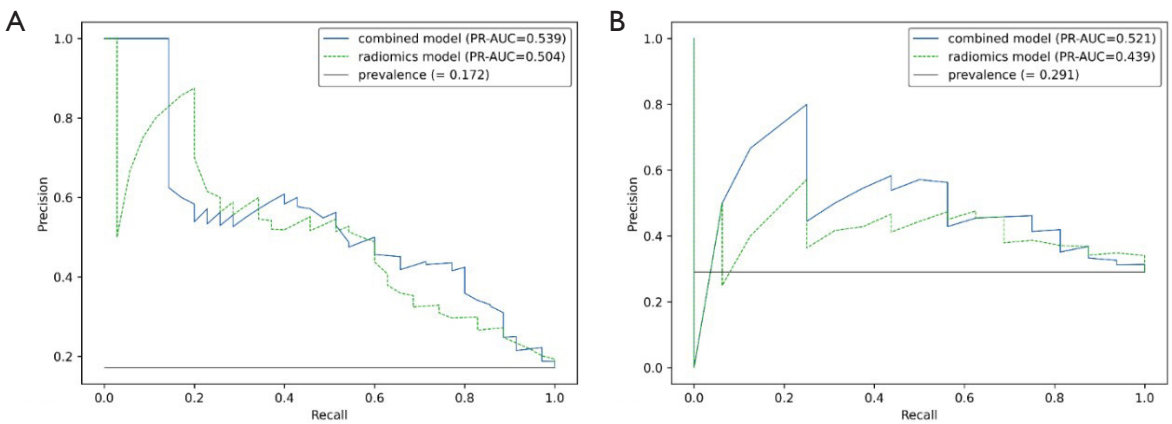

Figure S2 PR curves for the radiomics model and combined models in the training and validation sets. PR curves comparing the radiomics model and the combined model in the training set (A) and the validation set (B). The combined model consistently demonstrated higher PR-AUC than the radiomics-only model in both datasets. The horizontal black line represents the prevalence of HCC in each cohort. AUC, area under the receiver operating characteristic curve; HCC, hepatocellular carcinoma; PR, precision-recall; PR-AUC, precision-recall AUC.

https://dx.doi.org/10.21037/jgo-2025-aw-919

Table S1 Model specification of radiomics model

Variables	Coefficient (β)	Robust SE	Odds ratio (95% CI)	P value
Intercept	–2.735	0.921	–	0.003
Radiomics model (per 1-unit increase)	4.404	1.298	81.8 (6.42–1,042.60)	0.001

CI, confidence interval; SE, standard error.

Table S2 Model specification of combined model

Variables	Coefficient (β)	Robust SE	Odds ratio (95% CI)	P value
Intercept	–3.213	1.087	–	0.003
Radiomics model (per 1-unit increase)	4.322	1.324	75.31 (5.62–1,009.20)	0.001
Location (loc = 1 *vs.* 0)	0.938	0.391	2.55 (1.19–5.50)	0.016

CI, confidence interval; SE, standard error.

https://dx.doi.org/10.21037/jgo-2025-aw-919